JEM Journal of Experimental Medicine

BRIEF DEFINITIVE REPORT

Epidermal γδ T cells originate from yolk sac hematopoiesis and clonally self-renew in the adult

Rebecca Gentek[1*], Clément Ghigo[1*], Guillaume Hoeffel[1,2*], Audrey Jorquera[1], Rasha Msallam[2], Stephan Wienert[3], Frederick Klauschen[3], Florent Ginhoux[2,4], and Marc Bajénoff[1]

The murine epidermis harbors two immune cell lineages, Langerhans cells (LCs) and γδ T cells known as dendritic epidermal T cells (DETCs). LCs develop from both early yolk sac (YS) progenitors and fetal liver monocytes before locally self-renewing in the adult. For DETCs, the mechanisms of homeostatic maintenance and their hematopoietic origin are largely unknown. Here, we exploited multicolor fate mapping systems to reveal that DETCs slowly turn over at steady state. Like for LCs, homeostatic maintenance of DETCs is achieved by clonal expansion of tissue-resident cells assembled in proliferative units. The same mechanism, albeit accelerated, facilitates DETC replenishment upon injury. Hematopoietic lineage tracing uncovered that DETCs are established independently of definitive hematopoietic stem cells and instead originate from YS hematopoiesis, again reminiscent of LCs. DETCs thus resemble LCs concerning their maintenance, replenishment mechanisms, and hematopoietic development, suggesting that the epidermal microenvironment exerts a lineage-independent influence on the initial seeding and homeostatic maintenance of its resident immune cells.

Introduction

Mammalian hematopoiesis is a multi-step and multi-site process. Early hematopoiesis occurs in the extra-embryonic yolk sac (YS) and is restricted to few hematopoietic lineages. Between embryonic day (E) 7 and E10 of mouse development, YS hematopoiesis generates erythrocytes, megakaryocytes, macrophages, and mast cells (Palis et al., 1999; Orkin and Zon, 2008; Ginhoux et al., 2010; Gomez Perdiguero et al., 2015; Hoeffel et al., 2015; Mass et al., 2016; Gentek et al., 2018). Starting around E10, multipotent hematopoietic stem cells (HSCs) are produced in the major arteries of the mouse embryo, including the aorta-gonado-mesonephros region (Boisset et al., 2010). In the adult, HSCs colonize the bone marrow (BM) and are thought to generate all hematopoietic lineages (Sawai et al., 2016). While most immune cells exclusively derive from HSCs in the mouse, some lineages such as macrophages and mast cells are sequentially generated from YS progenitors and HSCs (Gomez Perdiguero et al., 2015; Hoeffel et al., 2015; Mass et al., 2016; Gentek et al., 2018).

Myeloid cells exhibit marked tissue residency, whereas the majority of lymphocytes is circulating between lymphoid sites. However, populations of $CD8^+$ memory T cells, innate-like lymphocytes such as innate lymphoid cells, and unconventional T cells, which include γδ T cells, also exhibit tissue residency primarily in barrier tissues, where they are thought to form a first line of defense against pathogens. One such tissue is the epidermis, the outermost layer of the skin that in mice harbors two resident immune cell populations: myeloid Langerhans cells (LCs) and lymphoid dendritic epidermal T cells (DETCs; Bergstresser et al., 1983). DETCs are intraepithelial γδ T cells that express a T cell receptor with the Vγ5 Vδ1 rearrangement and a restricted repertoire (Heilig and Tonegawa, 1986). DETCs modulate inflammation, protect against cutaneous neoplasia, and are implicated in skin wound healing (Girardi et al., 2002, 2003; Jameson et al., 2002; Sharp et al., 2005; Havran and Jameson, 2010; MacLeod et al., 2014). They develop from fetal thymic progenitors that seed the epidermis in low numbers before birth. Numbers of DETCs increase until adulthood is reached, after which they remain stable (Asarnow et al., 1988; Havran and Allison, 1988; Elbe et al., 1989; Havran et al., 1989; Payer et al., 1991; Jameson et al., 2004). However, the hematopoietic sources that generate these progenitors as well as the cellular mechanisms by which the DETC network is maintained once fully established are poorly characterized.

Here, we addressed the homeostatic maintenance mechanisms of DETCs and their hematopoietic origin using a combination of multicolor and hematopoietic fate mapping systems. We revealed that the adult DETC network undergoes slow homeostatic turnover mediated by tissue-resident proliferative units.

[1]Aix-Marseille University, Centre National de la Recherche Scientifique, Institut National de la Santé et de la Recherche Médicale, Centre d'Immunologie de Marseille-Luminy, Marseille, France; [2]Singapore Immunology Network, Agency for Science, Technology and Research, Singapore; [3]Institute of Pathology, Charité Universitätsmedizin Berlin, Berlin, Germany; [4]Shanghai Institute of Immunology, Shanghai JiaoTong University School of Medicine, Shanghai, China.

*R. Gentek, C. Ghigo, and G. Hoeffel contributed equally to this paper; Correspondence to Marc Bajénoff: bajenoff@ciml.univ-mrs.fr.

The same process, albeit enhanced, replenishes adult DETCs after injury. Thus, DETCs maintain and replenish through the same cellular mechanisms as LCs (Ghigo et al., 2013). In the light of these similarities, we hypothesized that DETCs and LCs might also have common developmental origins. Hematopoietic lineage tracing demonstrated that DETCs are established from YS hematopoiesis independently of definitive HSCs, indeed reminiscent of LCs. Epidermal DETCs and LCs thus share cellular dynamics and hematopoietic features, characteristics that are likely at least partially controlled by their microenvironment.

Results and discussion

The DETC network is composed of adjacent proliferative units

We first investigated the dynamics of DETC homeostasis in adulthood. In line with previous reports, we observed no contribution of transplanted BM to DETCs 3 mo after transplantation into mice that underwent full-body irradiation (Fig. 1 A and Fig. S1; Honjo et al., 1990; Sumaria et al., 2011). Similarly, DETCs remained exclusively of host origin in parabiotic mice (Fig. 1 B and Fig. S1), in which chimerism of circulating cells is achieved surgically through establishment of a joint circulation (Waskow, 2010; Kamran et al., 2013). Chimeric and parabiotic approaches therefore confirmed DETCs as tissue-resident cells that are radioresistant and maintain themselves independently of circulating progenitors under homeostatic conditions. These features were highly reminiscent of LCs and raised the possibility that DETCs do turn over in adult mice via local self-renewal, as shown for LCs (Merad et al., 2002; Hoeffel et al., 2012; Ghigo et al., 2013).

Tools that are now routinely used to track lymphocytes, such as intravital 2-photon microscopy, are inherently unsuited to resolve slow cellular dynamics that take days, weeks, or months, kinetics that likely apply to DETCs (Cahalan et al., 2002). Recombinase-driven multicolor fate mapping systems such as "Brainbow" mice, on the other hand, represent valuable tools to analyze cellular dynamics in situ (Livet et al., 2007; Hadjieconomou et al., 2011; Hampel et al., 2011; Ghigo et al., 2013; Pan et al., 2013; Mondor et al., 2016). These models enable clonal analysis in situ and thereby provide insights into cellular homeostasis and precursor-product relationships. The "Ubow" mouse is a derivative of the Brainbow model, in which the multicolor reporter cassette is under control of the human *UbiquitinC* (*Ubc*) promoter (Ghigo et al., 2013). This allows for combinatorial expression of three spectrally different fluorescent reporter proteins by Cre recombinase activity (Fig. 1 C). In the absence of Cre, Ubow cells ubiquitously express tdTomato. Upon Cre expression, cells perform a single and definitive recombination event that leads to the random acquisition of CFP and/or YFP, which is transmitted to their progeny. As DETCs express the fractalkine receptor CX3CR1 (Almeida et al., 2015), we intercrossed Ubow and *Cx3cr1*^{Cre} mice (Yona et al., 2013) to perform multicolor fate mapping of DETCs (Fig. 1, C–E). In *Cx3cr1*$^{Cre/wt}$ Ubow$^{+/+}$ mice, DETCs (identified as CD45$^+$ CD3$^+$ TCR Vγ5$^+$ MHCII$^-$) indeed expressed CFP and/or YFP (Fig. 1 C), indicating that they have undergone recombination of the Ubow construct. Although Cre-mediated recombination occurs in a stochastic fashion in Ubow mice, we consistently observed a bias toward YFP expression, as reported before (Ghigo et al., 2013). We took advantage of this bias by tracking the rare CFP$^{+/+}$ DETC population (on average 2.5% of all DETCs) to exemplify the behavior of the entire population. We thus investigated the arrangement of colored DETCs in the epidermis of adult *Cx3cr1*$^{Cre/wt}$ Ubow$^{+/+}$ mice by imaging. Confocal microscopy revealed that CFP$^{+/+}$ DETCs were, in fact, not randomly distributed in the epidermis but instead assembled in mono-colored foci (Fig. 1 D). This was confirmed by quantification of CFP$^{+/+}$ DETC clusters using "ClusterQuant" analysis, software that compares the experimentally observed assembly of colored cells in clusters with their computationally simulated random distribution (Ghigo et al., 2013). This approach indicated with high significance that CFP$^{+/+}$ DETCs form clusters (Fig. 1 E). Thus, like LCs, DETCs assemble in tissue-resident, proliferative units in the adult epidermis.

Homeostatic maintenance of adult DETCs relies on clonal proliferation

In *Cx3cr1*^{Cre} Ubow mice, recombination events are initiated as soon as DETCs express *Cx3cr1* during their development. These data therefore cannot delineate whether DETCs turn over constantly or if cluster formation is the result of transient expansion confined to a specific developmental stage followed by minimal homeostatic turnover in the adult, as has been reported for LCs and suggested for DETCs (Havran and Allison, 1990; Havran et al., 1991; Payer et al., 1991; Matsue et al., 1993; Chorro et al., 2009). To estimate the extent of homeostatic DETC turnover in adult mice, we measured the incorporation of BrdU by DETCs over several weeks. LCs gradually incorporated BrdU over time, and after 5 wk, ∼20% of them were labeled (Fig. 2 A; Kamath et al., 2002). On the contrary, the cumulative fraction of BrdU-labeled DETCs reached only 2% over this period, confirming that adult DETCs are cycling very slowly at steady state (Fig. 2 A; Sumaria et al., 2011).

To track this slow homeostatic turnover, we turned to a model in which Ubow recombination can be induced in adult DETCs. We generated *Cx3cr1*$^{CreERT2/wt}$ Ubow$^{+/+}$ mice (Chorro et al., 2009; Yona et al., 2013). In these mice, injection of a low dose of tamoxifen induces recombination in some DETCs, as a consequence of which they stochastically acquire expression of CFP and/or YFP, hence generating an initial mosaic of colored DETCs. We reasoned that longitudinal analysis of tamoxifen-treated *Cx3cr1*$^{CreERT2/wt}$ Ubow$^{+/+}$ mice should unravel any slow homeostatic DETC turnover occurring in the adult. As BM-derived cells do not contribute to adult DETC homeostasis, we reasoned that every dying DETC should be replaced by a tissue-resident one. If DETCs were capable of replacing their dying neighbors by local proliferation, mono-colored foci composed of dividing DETCs and their progeny should develop over time. 1 wk after tamoxifen administration to adult mice, ∼6–7% of DETCs had undergone recombination and were randomly distributed (Fig. 2, B–D). Analysis of DETC cluster formation in adult *Cx3cr1*$^{CreERT2/wt}$ Ubow$^{+/+}$ mice up to 6 mo after tamoxifen treatment revealed that the initial mosaic of CFP$^{+/+}$, YFP$^{+/+}$, and CFP$^+$YFP$^+$ DETCs was indeed progressively replaced by rare foci of mono-colored DETCs similar to the ones observed in constitutive *Cx3cr1*$^{Cre/wt}$ Ubow$^{+/+}$ mice (Fig. 1 and Fig. 2, C and D).

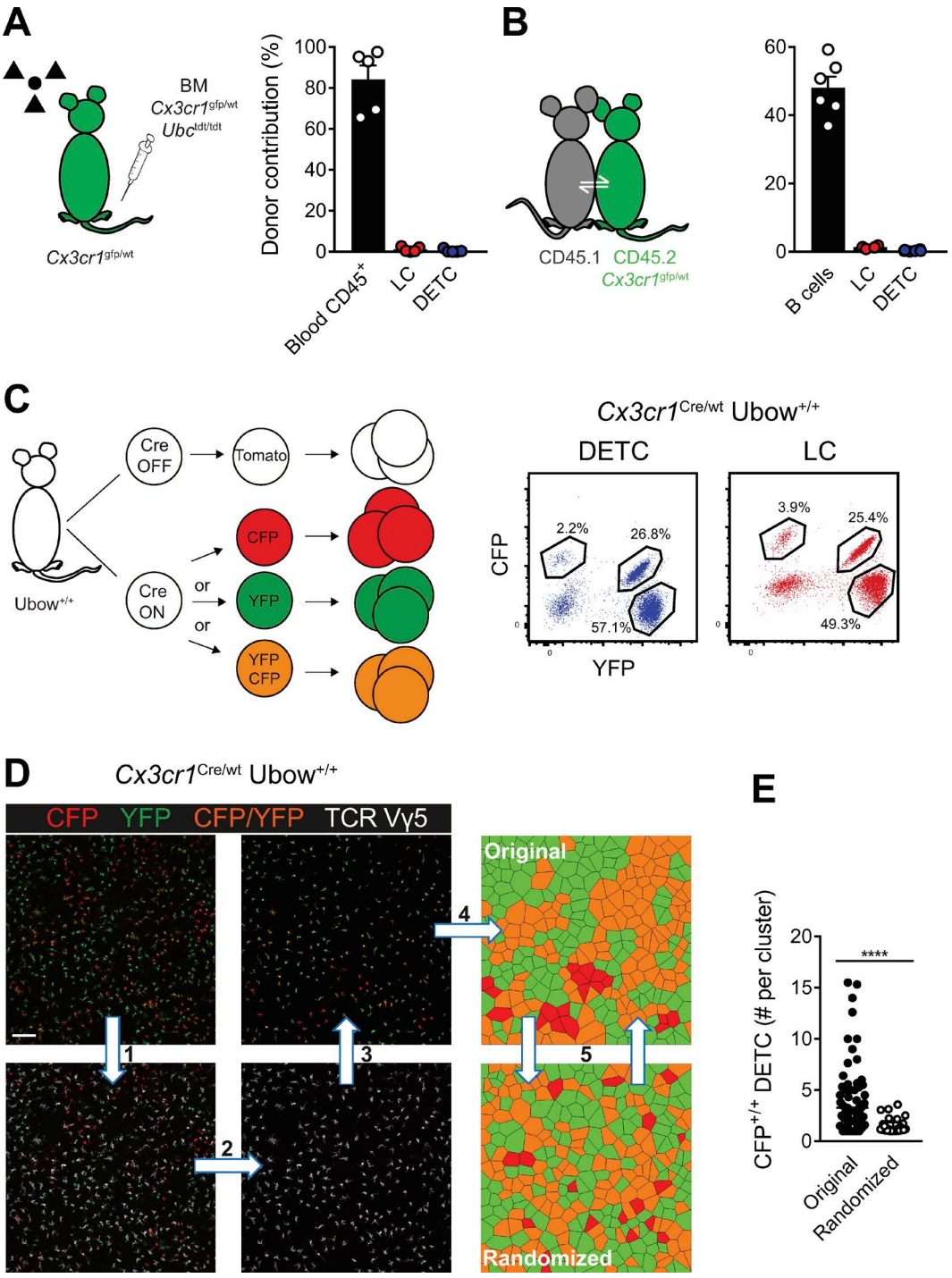

Figure 1. **Adult DETCs assemble in clonal units. (A)** *Cx3cr1*$^{gfp/wt}$ mice were lethally irradiated and reconstituted with BM from *Cx3cr1*$^{gfp/wt}$ *Ubc*$^{tdt/tdt}$ mice. 3 mo later, the contribution of tdTomato$^+$ donor BM to DETCs (TCR Vγ5$^+$ CD3$^+$) and LCs (F4/80$^+$ MHCII$^+$) was assessed by flow cytometry. To assess total reconstitution levels by donor BM, circulating blood leukocytes (blood CD45$^+$) were analyzed as controls. Data are pooled from three independent experiments with one or two individual mice per experiment. **(B)** CD45.1 WT and CD45.2 *Cx3cr1*$^{gfp/wt}$ mice were surgically joined. After 2 mo, the origin of DETCs and LCs was determined by flow cytometry. This origin is expressed as the relative contribution of CD45.1$^+$ or CD45.2$^+$ nonhost cells to the individual parabionts of the respective other genotype. Lymph node B cells served as controls for the establishment of a shared circulation. Three parabiotic pairs were analyzed. Data in A and B are displayed as mean (columns) ± SEM (error bars), with data points corresponding to individual mice. **(C–E)** Multicolor fate mapping of DETCs in Ubow$^{+/+}$ mice. **(C)** Left: In the absence of Cre, all cells express tdTomato. Upon Cre activity, cells lose tdTomato expression and stochastically acquire YFP or CFP. This choice is definitive and transmittable to the progeny of the Cre-expressing cells. Right: Flow cytometric analysis of DETCs and LCs harvested from the epidermis of *Cx3cr1*$^{Cre/wt}$ Ubow$^{+/+}$ mice. Cells were pregated as CD45$^+$ and TCR Vγ5$^+$ (DETC) or MHCII$^+$ (LC). **(D and E)** Confocal imaging analysis of DETC clusters in *Cx3cr1*$^{Cre/wt}$ Ubow$^{+/+}$ mice. Epidermal sheets were stained for TCR Vγ5 (step 1). Fluorescent signals corresponding to TCR Vγ5$^+$ DETCs were digitally isolated using Imaris Image Analysis software (step 2). This enables analysis of fluorescent reporter recombination in DETCs only (step 3). The resulting confocal images were then digitally rendered into voronoi tessellated pictures (step 4) that are amenable to computational simulation. The number of CFP$^{+/+}$ DETCs per cluster was determined in the experimental data ("original") and compared with Monte Carlo simulations in which DETCs were randomly distributed (step

Collectively, these data uncovered that the adult DETC network does slowly turn over at steady state. This turnover is achieved through local self-renewal, resulting in clonal units comprised of proliferating DETCs and their progeny. Such cellular dynamics are highly reminiscent of LCs, whose homeostasis also relies on clonal proliferative units (Ghigo et al., 2013). However, this process is considerably slower for DETCs, taking several months to be detectable in the Ubow system. These distinct turnover rates probably reflect differences in the frequency with which these cell types need to be replaced. Indeed, LCs, but not DETCs, continuously migrate from the epidermis to skin draining lymph nodes, both under inflammatory conditions and at steady state (Merad et al., 2008). Such constant need for partial replenishment of the LC network likely explains their higher turnover (Merad et al., 2002; Chorro et al., 2009). The low-grade clonal self-renewal of DETCs, on the other hand, might serve to replace the few DETCs dying over time.

Accelerated local proliferation replenishes the damaged DETC network

The magnitude of and mechanisms underlying DETC turnover might be different, however, when homeostasis is perturbed. To investigate whether local self-renewal is also involved in the maintenance and replenishment of the DETC network under conditions of tissue injury, we used tape stripping (TS), a model in which the repeated application of adhesive tape to the ear induces epidermal abrasion and an inflammatory response (Holzmann et al., 2004; Strid et al., 2011). We first subjected WT mice to TS and measured the proliferation of DETCs at the peak of inflammation (10 d) and when the epidermis had been repaired (30 d) using 5-ethynyl-2′-deoxyuridine (EdU) incorporation (Fig. 3 A). TS induced enhanced LC and DETC proliferation at the peak of inflammation, with 6% of DETCs in S-phase compared with 1% in untreated control epidermis. After 30 d, DETC proliferation had returned to baseline. To address whether DETC restoration following injury was also supported by the mobilization of BM-derived progenitors, we performed TS on BM chimeric mice (Fig. 3 B). As previously observed (Ghigo et al., 2013), BM-derived cells engrafted in the LC network of the repaired epidermis at low frequency. DETCs, on the other hand, did not receive any BM contribution by 30 d after TS. Together, these results demonstrate that DETCs locally respond to injury with a transient increase in proliferation.

To directly test whether this seemingly autonomous DETC replenishment following injury was mediated by local clonal proliferation, we analyzed cluster formation in adult tamoxifen-treated *Cx3cr1*$^{CreERT2/wt}$ Ubow$^{+/+}$ mice that were then subjected to TS of one ear (Fig. 3, C and D). Confocal imaging revealed that DETCs assembled in clusters already 1 mo later in TS but not untreated control ears. These findings were in line with the enhanced proliferative response observed by EdU incorporation and indicate that clonal self-renewal replenishes the DETC network upon perturbation. Hence, DETC homeostasis and replenishment seem to depend on similar cellular strategies.

At steady state, DETCs are polarized, immotile cells that possess anchored projections at keratinocyte tight junctions (Chodaczek et al., 2012). However, DETCs are known to round up following wounding and could thus reacquire motility, migrate, and proliferate to replenish the damaged epithelial network in a distant location (Havran and Jameson, 2010; Strid et al., 2011). Therefore, an alternative, albeit not mutually exclusive, mechanism by which the damaged DETC network could be replenished independently from peripheral progenitors is through relatively long-range migration and subsequent proliferation of DETCs (progenitors) from distant unperturbed locations, a possibility that our experiments do not formally exclude.

To assess migration of DETCs in epidermal wounding, we established skin grafts, in which a piece of WT skin was grafted onto the back of *Cx3cr1*$^{gfp/wt}$ *Ubc*^{tdt} mice (Fig. 3 E). In this model, host DETCs can be identified by virtue of their GFP expression, while the graft border is visible from the mismatch between ubiquitously tdTomato-expressing host cells and the nonfluorescent graft. Whole mount confocal imaging 4 mo after grafting revealed that host DETCs were only found in the graft within 600 µm of the border and constituted a sizeable fraction of 10–20% only within 300 µm. Taking into account the total graft size of ∼10 mm × 15 mm, host DETCs were thus mostly restricted to the immediate edge of the wound. These data therefore argue against long-range migration of DETCs and favor a model in which the DETC network in damaged epidermis is primarily restored through proliferation of neighboring DETCs or their progenitors.

DETCs originate from HSC-independent YS hematopoiesis

Overall, DETCs and LCs display striking similarities: both are tissue-resident cells occupying the epidermis, where they form comparably dense networks of radioresistant cells that self-maintain independently of input from the BM and circulating progenitors. At steady state, both networks are dynamic structures composed of adjacent proliferative units. Clonal proliferation is also the major mechanism by which DETCs and LCs are replenished upon perturbation, albeit at different frequencies. Intriguingly, DETCs and LCs also share some developmental characteristics: both lineages depend on the transcription factor Runx3, and, as outlined above, although they continue to mature in the perinatal period in terms of their phenotype and numbers, both networks are established prenatally (Havran and Allison, 1990; Payer et al., 1991; Elbe et al., 1992; Fainaru et al., 2004, 2005; Woolf et al., 2007; Hoeffel et al., 2012). Indeed, neither LCs nor DETCs showed any contribution of transplanted BM in the epidermis of adult mice that had been shield-irradiated as newborns (Fig. 4 A), a model that allows BM engraftment under relatively unperturbed conditions in this developmental window (Scott et al., 2016; Baratin et al., 2017). Considering these similarities, we hypothesized that DETCs and LCs might also share hematopoi-

5; 1 of 10,000 simulations displayed). For further explanations, see Materials and methods section. ***, P < 0.0001, calculated using a nonparametric test (Mann–Whitney). Data in C–E are representative of five different experiments with two mice per experiment. Bars, median. Scale bar, 100 µm. For details on digital rendering and analysis of cluster formation, see Materials and methods section.

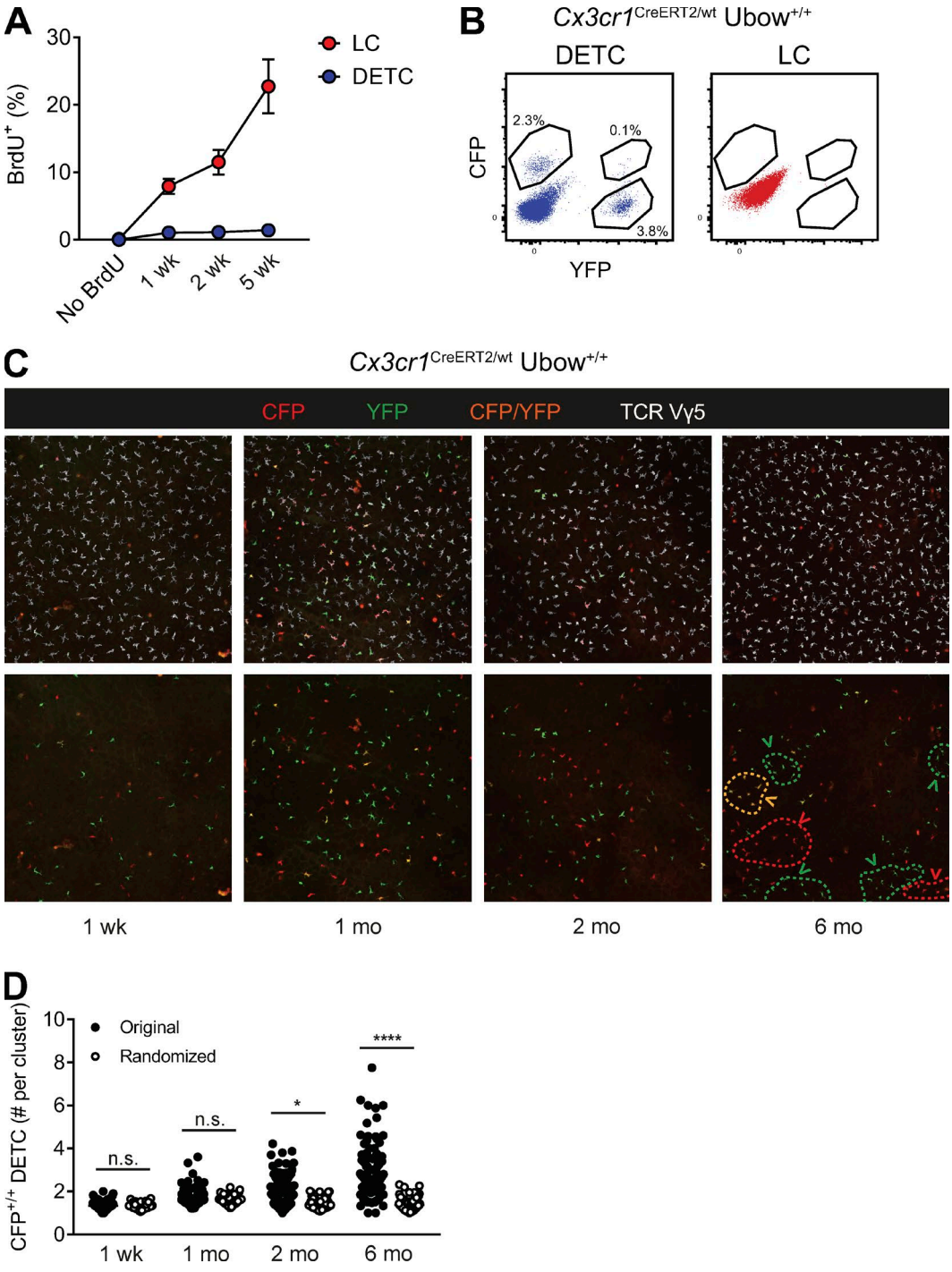

Figure 2. **DETCs clonally proliferate at steady state. (A)** Homeostatic turnover of DETCs and LCs. WT mice were provided with BrdU in their drinking water for the indicated duration. BrdU incorporation was quantified by flow cytometry at the indicated time points. Pooled data from two independent experiments (20 mice per experiment, 5 mice per time point) are shown as mean (symbols) ± SEM (error bars; B–D). Adult *Cx3cr1*$^{CreERT2/wt}$ Ubow$^{+/+}$ mice were administered a single dose of tamoxifen. **(B)** Cre-mediated recombination of fluorescent reporters by DETCs and LCs was determined by flow cytometry 1 wk after tamoxifen treatment. **(C and D)** Confocal imaging analysis of reporter recombination in TCR Vγ5^{+} DETCs of *Cx3cr1*$^{CreERT2/wt}$ Ubow$^{+/+}$. Epidermis was harvested 1 wk or 1, 2, or 6 mo after tamoxifen treatment. Top: Raw confocal images showing TCR Vγ5 staining and CFP/YFP fluorescence in all epidermal cells. Bottom: Fluorescent reporter signals corresponding to DETCs only (i.e., for digitally isolated TCR Vγ5^{+} DETCs (see steps 1–3 in Fig. 1). Arrowheads and dashed lines indicate mono-colored foci of DETCs. **(D)** Quantification of C. Numbers of CFP$^{+/+}$ DETCs per DETC foci were determined experimentally ("Original") and compared with computer-simulated random distribution ("Randomized") as in Fig. 1. Data in B–D are representative of two independent experiments (12 mice per experiment, 3 mice per time point). Bars in D, median. n.s., not significant; *, P < 0.05; ****, P < 0.0001, calculated using a nonparametric test (Mann–Whitney).

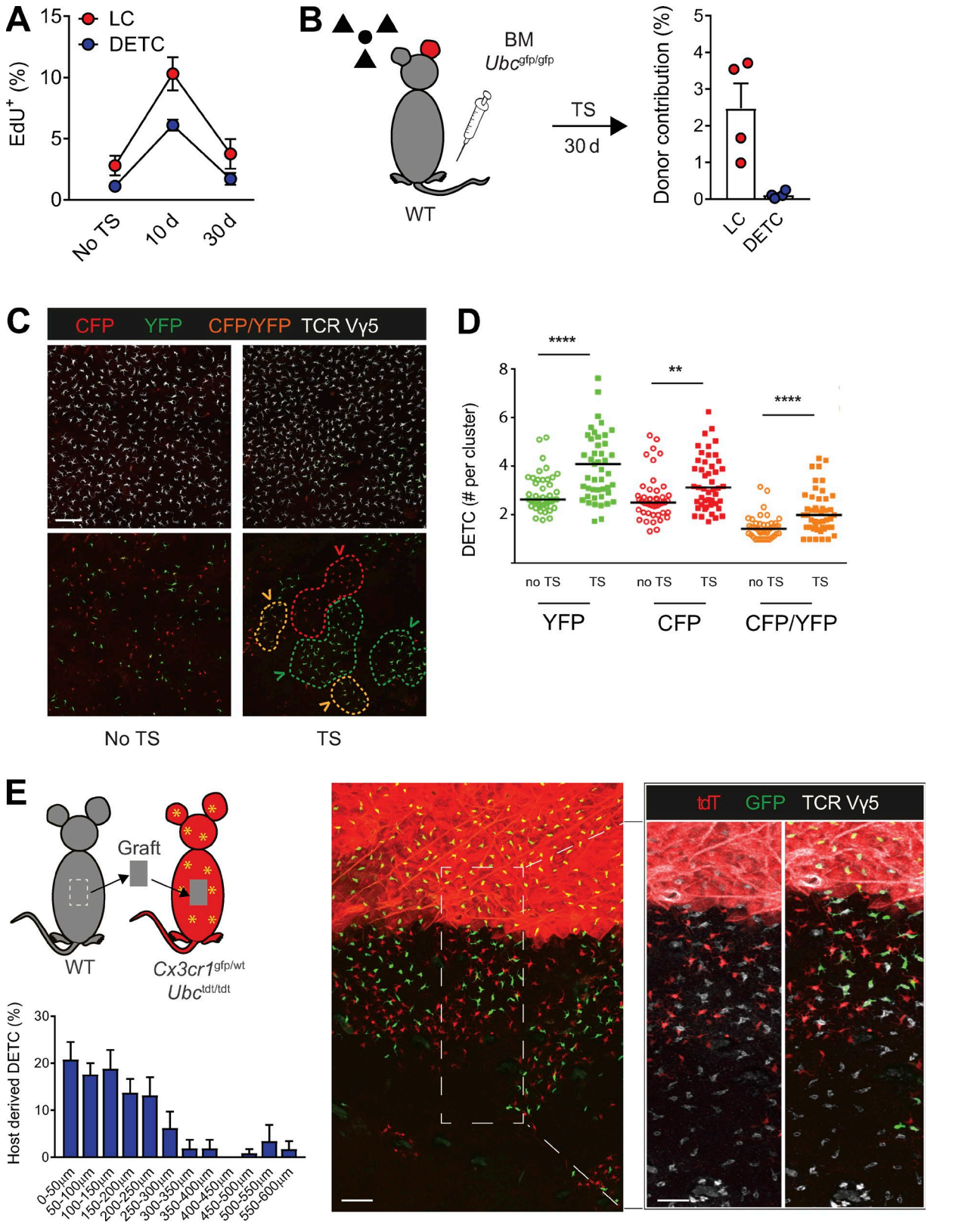

Figure 3. **Accelerated local self-renewal facilitates DETC replenishment following skin wounding. (A–D)** Sources of DETCs following TS. The left ears of WT mice (A), chimeras previously reconstituted with *Ubc*$^{gfp/gfp}$ BM (B), and *Cx3cr1*$^{CreERT2/wt}$ Ubow$^{+/+}$ mice (C and D) were tape stripped (TS). Contralateral ears served as controls (no TS). **(A)** 10 and 30 d after TS, mice were injected with EdU, and the percentages of EdU$^+$ DETCs and LCs were assessed 14 h later by flow cytometry. Data are pooled from three independent experiments with three mice each and displayed as mean (symbols) ± SEM (error bars). **(B)** Contribution of GFP$^+$ donor BM-derived cells to DETCs and LCs 30 d after TS. Data are derived from two independent experiments and shown as mean (columns) ± SEM (error bars). **(C and D)** *Cx3cr1*$^{CreERT2/wt}$ Ubow$^{+/+}$ mice received 1 mg tamoxifen and were tape stripped 1 wk later. The formation of mono-colored DETC clusters in tape

etic characteristics. The majority of LCs derives from fetal liver monocytes recruited to the skin starting around E14.5, while the remainder originates from progenitors produced by early YS hematopoiesis (Hoeffel et al., 2012). DETCs are established from fetal thymic progenitors that settle in the epidermis at mid- to late gestation, similar to LC precursors (Elbe et al., 1989, 1992; Havran and Allison, 1990; Payer et al., 1991).

Unlike for LCs, however, the hematopoietic source of these progenitors, and by extension of adult DETCs, has not been identified yet. We sought to address the ontogeny of DETCs using genetic fate mapping. We recently established that *Cdh5*-CreERT2 mice can be used to efficiently and precisely label either early YS- or HSC-dependent definitive hematopoiesis in a temporally defined manner (Gentek et al., 2018). This model exploits the fact that *Cdh5* (encoding VE-cadherin) is expressed by endothelial cells, but down-regulated immediately upon endothelial-to-hematopoietic transition (Breier et al., 1996; Zovein et al., 2008). In *Cdh5*-CreERT2 Rosa^{tdt} mice, administration of a single dose of 4-hydroxytamoxifen (4OHT) at defined embryonic time points therefore labels hemogenically active endothelial cells and fate maps their hematopoietic output. Specifically, 4OHT treatment at E7.5 labels the hemogenic endothelium of the YS and its early output, including microglia. Administration of 4OHT at E10.5, on the other hand, labels the hemogenic endothelium of the aorta-gonado-mesonephros and consequently, definitive HSCs and their progeny such as adult circulating leukocytes, but not microglia (Gentek et al., 2018; Fig. 4 B). Using this model, we found that the epidermis of adult *Cdh5*-CreERT2$^{+/wt}$ Rosa$^{tdt/wt}$ mice contains a minor but sizeable population of E7.5-labeled DETCs generated by early YS hematopoiesis (Fig. 4 B). Unlike LCs, however, adult DETCs showed only marginal E10.5 labeling, indicating that they do not originate from adult-type, HSC-dependent definitive hematopoiesis. These findings were confirmed in *Runx1*$^{CreERT2/wt}$ Rosa$^{yfp/wt}$ mice, in which 4OHT administration at E7.5 fate maps early YS hematopoiesis, while pulsing at E9.5 primarily fate maps HSC-dependent definitive hematopoiesis (Ginhoux et al., 2010; Hoeffel et al., 2012, 2015; Fig. 4 C). Thus, while early YS hematopoiesis marginally contributes to adult DETCs, the majority of DETCs originates from neither early YS progenitors nor definitive HSC-dependent hematopoiesis.

While seemingly surprising, these findings are in line with the recruitment of progenitors with T cell potential to the thymus anlagen as early as E11 (Jotereau et al., 1987; Masuda et al., 2005; Bell and Bhandoola, 2008). Irrespective of whether they represent the extreme of a continuum or a truly distinct wave, the majority of DETCs could be produced by late YS hematopoiesis. In support of this hypothesis, DETCs were fate mapped to a similar degree as LCs in *Runx1*$^{CreERT2/wt}$ Rosa$^{yfp/wt}$ mice treated with 4OHT at E8.5, an approach that primarily labels the output of late YS, but not early YS and definitive hematopoiesis (Hoeffel et al., 2015; Fig. 4 C). Unlike LCs, however, DETCs never showed any contribution of cells labeled with 4OHT in *Csf1r*^{CreERT2} Rosa$^{yfp/wt}$ mice, a model known to label erythro-myeloid progenitors generated by HSC-independent YS hematopoiesis, which contribute to the first wave of LCs (Gomez Perdiguero et al., 2015; Hoeffel et al., 2015; Fig. 4 D). Thus, although they share developmental kinetics, DETCs and LCs are established from distinct progenitors.

Several candidates exist for such DETC progenitors. A recent study identified a population of embryonic "developmentally restricted HSCs" that exhibits marked differentiation bias toward tissue resident innate-like lymphocytes, including TCR Vγ5$^+$ T cells. Furthermore, progenitors with lymphoid and lymphomyeloid potential have been described in the YS (Palacios and Imhof, 1993; Yoshimoto et al., 2012; Böiers et al., 2013). Such progenitors are not endowed with long-term reconstitution capacity. However, once seeded in their tissue of residency, their progeny could be maintained by local self-renewal throughout life. This would be in agreement with the mode of homeostatic maintenance we unraveled here for adult DETCs. Based on these considerations and our fate mapping data, we conclude that DETCs are produced by YS hematopoiesis. To our knowledge, this makes DETCs the only lymphoid lineage with identified YS origin. Much like their adult maintenance and replenishment mechanisms, their developmental origin closely resembles that of LCs, with which they co-occupy the epidermis. This suggests that in addition to lineage-specific factors like IL-34 for LCs and IL-2 and IL-15 for DETCs, other factors produced by, e.g., keratinocytes might regulate local development and maintenance of both DETCs and LCs (Ye et al., 2001; Greter et al., 2012; Wang et al., 2012).

In summary, our study demonstrated that adult DETCs undergo slow homeostatic turnover and identified clonal self-renewal as the underlying cellular mechanism. The same mechanism, albeit accelerated, is responsible for replenishing the DETC network following injury. DETCs therefore bear striking resemblance to LCs that reside in the same environment. Moreover, we revealed that DETCs and LCs also share an origin from HSC-independent YS hematopoiesis that, within lymphocytes, is unique to DETCs. Collectively, these data suggest that the microenvironment imposes a dominant degree of regulation on its resident immune cells, independently of their lineage identity. Whether such environmental imprinting also applies to other tissues should be subject to future studies.

Materials and methods

Ethics statement and mouse lines

Mice housed at the Centre d'Immunologie de Marseille-Luminy (Marseille, France) were maintained under specific pathogen–free conditions in a 12-h light/dark cycle at an ambient temperature of 22°C. Animals were kept in individually ventilated

stripped and control ears was analyzed 1 mo later by confocal microscopy (C) and quantified as in Figs. 1 and 2 (D). Bars, mean. Error bars, SEM. Arrowheads and dashed lines in C indicate mono-colored DETCs. Scale bar, 100 µm (C). **, P < 0.01; ****, P < 0.0001, calculated with the nonparametric Mann–Whitney test. **(E)** Skin from nonfluorescent WT donors was grafted on the back of *Cx3cr1*$^{gfp/wt}$ *Ubc*$^{tdt/tdt}$ mice. After 4 mo, the frequency of GFP$^+$ TCR Vγ5$^+$ host DETCs within the grafted skin was determined at various distances from the wound edge. Bars, mean + SEM. Representative confocal images (right) and quantification (left, bottom) of three independent experiments are shown. Scale bars, 70 µm (left); 40 µm (right).

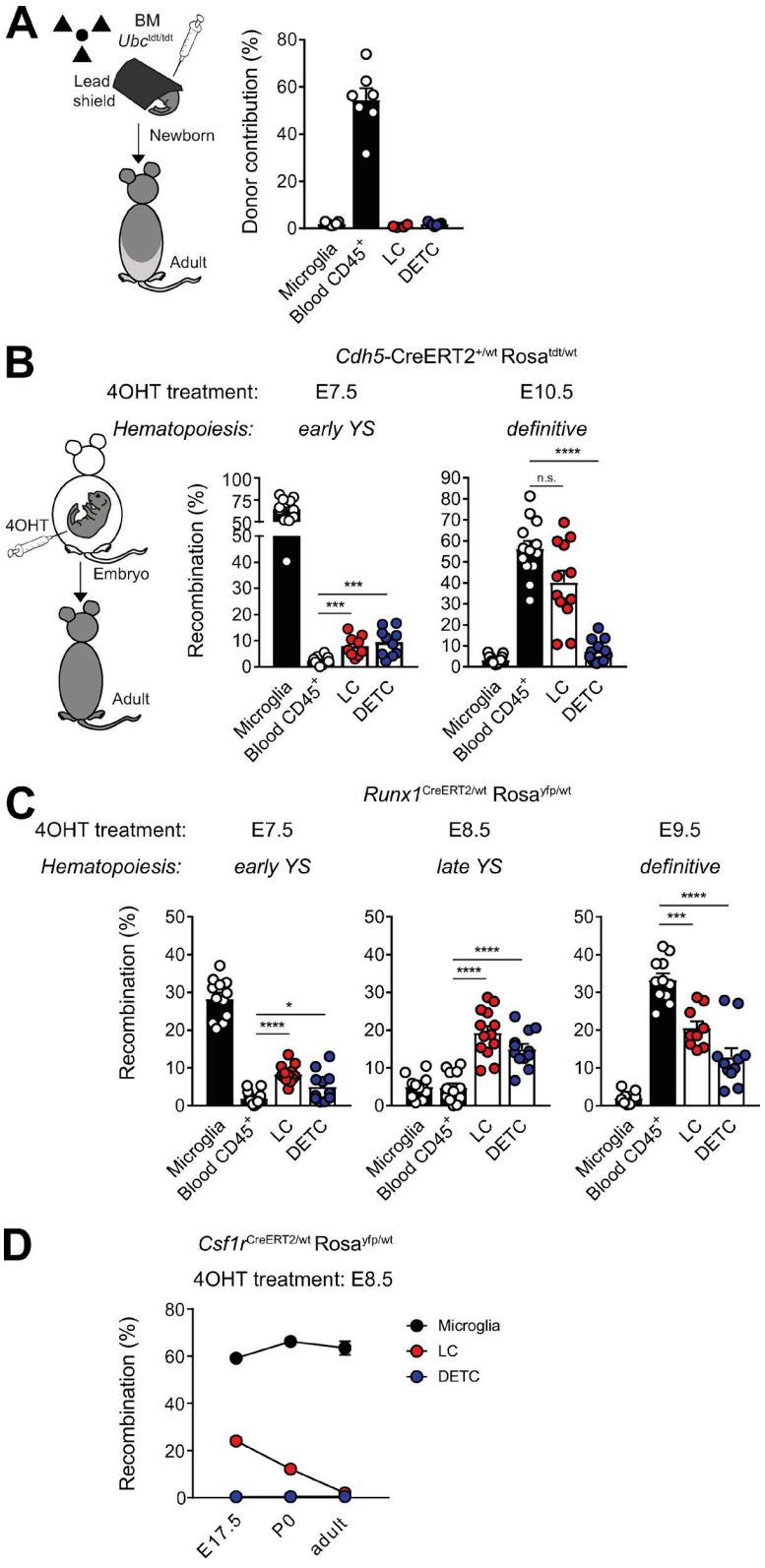

Figure 4. **DETCs develop from HSC-independent YS hematopoiesis. (A)** WT mice were shield-irradiated as newborns and transplanted with CD11b-depleted BM from *Ubc*$^{tdt/tdt}$ donors, and the contribution of the grafted BM to DETCs and LCs was analyzed by flow cytometry when mice had reached adulthood. Donor contribution to brain microglia and circulating leukocytes was analyzed as references for efficacy of shielding and engraftment, respectively. **(B–D)** *Cdh5*-CreERT2$^{+/wt}$ Rosa$^{tdt/wt}$ (B), *Runx1*$^{CreERT2/wt}$ Rosa$^{yfp/wt}$ (C), and *Csf1r*$^{CreERT2/wt}$ Rosa$^{yfp/wt}$ (D) mice were administered a single dose of 4OHT in utero at the indicated time points. Fluorescent reporter recombination was assessed in DETCs and LCs of adult mice (B and C) or at the indicated ages (D). All data are pooled from minimally two independent experiments (litters) and depicted as mean (columns) + SEM (error bars), with single data points corresponding to individual mice (B and C) or mean (symbols) ± SEM (error bars; D). Microglia and circulating leukocytes served as controls for fate mapping of the output of YS (microglia) and adult-type definitive (blood CD45$^+$) hematopoiesis, respectively. n.s., not significant; *, P < 0.05; ***, P < 0.001; ****, P < 0.0001, derived from a nonparametric test (Mann–Whitney).

cages equipped with sterile quarter-inch corncob bedding and cotton pads for environmental enrichment. They were fed with irradiated standard pellet chow and reverse osmosis water. Experiments were performed in accordance with French and European guidelines for animal care under the permission no. 5–01022012 following review and approval by the local animal ethics committee in Marseille, France. Mice were on a C57BL/6J background (minimally eight backcrosses) and used between 6 and 12 wk of age, unless stated otherwise. *Cx3cr1*^{Cre} (B6J.B6N(Cg)-Cx3cr1$^{tm1.1(cre)Jung}$/J, strain 25524; Jung et al., 2000), *Cx3cr1*^{CreERT2} (B6.129P2(C)-Cx3cr1$^{tm2.1(cre/ERT2)Jung}$/J, strain 20940; Yona et al., 2013), *Ubc*^{gfp} (UBC-GFP 30Scha/J, strain 4353), and

Rosa^{tdt} (also known as Ai14, strain 7914; Madisen et al., 2010) were purchased from The Jackson Laboratory. C57BL/6J (WT), CD45.1 (CD45.1 WT), and RjOrl:SWISS (CD1) mice were from Janvier Labs. *Ubc*^{tdt} (Ubow) mice were generated at the Service des Animaux Transgéniques (Orléans, France) as described previously (Ghigo et al., 2013). *Cdh5*-CreERT2 mice (Sörensen et al., 2009) were a gift from Ralf Adams (Max Planck Institute for Molecular Biomedicine, Muenster, Germany). Experiments using *Runx1*^{CreERT2} (Samokhvalov et al., 2007) and *Csf1r*^{CreRT2} mice (The Jackson Laboratory) were performed at the Singapore Immunology Network (Singapore) following approval by the local ethics committee.

Parabiosis

10-wk-old WT CD45.1 and *Cx3cr1*$^{gfp/wt}$ CD45.2 mice were surgically joined as described previously (Waskow, 2010). Parabionts were analyzed 2 mo later.

Bone marrow (BM) chimeras

To generate regular BM chimeras, mice were subjected to full-body irradiation using an x-ray source and a total dose of 7 Gy. Mice were then reconstituted with at least 5 × 10^6 BM cells prepared using standard procedures. For shielded newborn chimeras, newborn mice were placed in a 6-mm-thick lead shield that only left their hind legs exposed while protecting the rest of the body from irradiation. Mice were reconstituted intravenously with 3 × 10^7 BM cells depleted of CD11b$^+$ cells through negative magnetic selection.

Timed pregnancies and in utero tamoxifen administration for fate mapping

Cdh5-CreERT2 fate mapping was performed as in Gentek et al. (2018). Briefly, timed matings were set up between WT females aged 6–10 wk and *Cdh5*-CreERT2$^{+/wt}$ Rosa$^{tdt/tdt}$ or *Cdh5*-CreERT2$^{+/+}$ Rosa$^{tdt/tdt}$ males. The presence of vaginal plugs was assessed the morning after, which was considered 0.5 d after conception. To induce reporter recombination in the offspring, a single dose of 4-hydroxytamoxifen (4OHT) was delivered by i.p. injections to pregnant females at E7.5 or E10.5. 4OHT solutions were supplemented with progesterone to counteract adverse effects of 4OHT on pregnancies. Females received a dose of 1.2 mg 4OHT and 0.6 mg progesterone. In cases when females could not give birth naturally, pups were delivered by C-section and cross fostered with lactating CD1 females. *Runx1*^{CreERT2} and *Csf1r*^{CreRT2} fate mapping experiments were performed at the Singapore Immunology Network (Singapore) as described previously (Hoeffel et al., 2015). Fate mapped *Cdh5*-CreERT2$^{+/wt}$ Rosa$^{tdT/wt}$ and *Runx1*$^{CreERT2/wt}$ Rosa$^{yfp/wt}$ mice were analyzed in the adult, and an analysis time course was performed for *Csf1r*^{CreRT2} mice. Statistical significance was assessed by an unpaired, nonparametric *t* test (Mann-Whitney).

Tamoxifen treatment of adult mice

Adult *Cx3cr1*$^{CreERT2/wt}$ Ubow$^{+/+}$ mice received a single dose of tamoxifen (1 mg) dissolved in corn oil (both Sigma-Aldrich) by i.p. injection.

In vivo BrdU and EdU incorporation assays

For longitudinal analysis of BrdU incorporation, mice were administered BrdU in their drinking water for up to 4 wk, the maximal possible duration due to BrdU toxicity, similar to what has previously been published for LCs (Merad et al., 2002). BrdU incorporation was detected using a BrdU Flow cytometry kit (BD Biosciences) following the manufacturer's protocol. To quantify cells currently in S-phase, EdU incorporation assays were performed. Mice were injected i.p. with 1 mg of EdU and sacrificed 14 h later. Epidermal DETCs and LCs were enriched using CD45 microbeads (Miltenyi Biotec), and EdU incorporation was detected using the Click it EdU flow cytometry kit (Life Technologies) according to the manufacturer's instructions.

Skin tape stripping (TS)

Mice were anesthetized with ketamine/xylazine. The dorsal side of the left ear was stripped by repeated application (15 times) of tape (3M comply indicator tape, 18 mm).

Skin grafts

Recipient mice were anesthetized with ketamine/xylazine. A single piece of back skin (~1 cm × 1.5 cm) was grafted in the center of the dorsal region of the recipient. Mice were treated with ibuprofen for 1 mo following surgery. Bandages were removed 7 d after surgery, and graft integrity was observed weekly.

Flow cytometry

Cell suspensions were obtained through mechanical dissociation and enzymatic digest. Briefly, brain and epidermis samples were harvested, finely minced with scissors, and digested in RPMI medium (Invitrogen) containing 0.1 mg/ml DNase I (Sigma-Aldrich) and 400 U/ml Collagenase I (Gibco). Epidermis was harvested from the ear skin. Briefly, dorsal and ventral sheets were separated using forceps, and the epidermis was removed by incubation in Dispase in PBS for 1 h at 37°C before digestion. Digests were performed for 30–45 min at 37°C under continuous agitation (900 rpm), and samples were regularly pipetted up and down to support mechanical dissociation and digest. Blood was drawn from the retro-orbital vein, and red blood cell lysis was performed before staining. Digested tissue samples were filtered, and single-cell suspensions were stained with fixable live dead stains (BioLegend), blocked in a suspension containing normal rat (Jackson ImmunoResearch) and mouse serum (Thermo Fisher Scientific) and anti CD16/32 ("TruStain Fx"; BioLegend). Surface staining was performed in FACS buffer supplemented with Brilliant Stain Buffer (BD Biosciences) for 20–30 min at 4°C. Data were acquired on LSRII and LSR Fortessa X-20 instruments (BD Biosciences) and analyzed using FlowJo (Treestar) and Prism (GraphPad) software.

Immunostaining and confocal microscopy

To prepare epidermal sheets, the dorsal and ventral halves of ear skin were pulled apart as for flow cytometry and incubated in Dispase for 40 min. Epidermal sheets were separated from the dermis, fixed in AntigenFix (Microm Microtech) for 20 min at room temperature, and washed in phosphate buffer. DETCs were identified by immunostaining TCR Vγ5 expression. Immunoflu-

orescence confocal microscopy was performed with a Zeiss LSM 780 confocal microscope. Final image processing was performed with Imaris software (Bitplane) and Adobe Photoshop.

Antibodies and reagents

In addition to critical reagents listed throughout this section, the following antibodies were used for flow cytometry and confocal imaging: anti–mouse CD45 (30-F11; BD Biosciences), CD3 (17A2; BioLegend), TCR Vγ5 (536; BioLegend), MHCII (M5/114.15.2; eBioscience), F4/80 (BM8; BioLegend), CD64 (X54-5/7.1; BioLegend), CD11b (M1/70; BioLegend), and Ly6C (AL-21; BD Biosciences).

Quantification of DETC clusters

Quantification and statistical analysis of the spatial distribution of DETCs consist of three modules combined in the ClusterQuant software, which we developed with the CognitionMaster image analysis platform based on C#/.NET. In the first module, DETC classes are defined using the Region-of-Interest plugin (ROImanager) of ClusterQuant/CognitionMaster. The respective cells are labeled manually to obtain the cell center coordinate information for the subsequent processing step. The second module computes a two-dimensional Voronoi mesh based on the manually labeled cell centers. The resulting tessellation establishes the neighborhood relationship between the cells, which is used to evaluate the number of same-type cells assembled in clusters as well as the respective cluster size. This step provides a robust and objective means of cell cluster quantification. To assess the degree of randomness of the observed cell distribution/cluster formation, Monte Carlo simulations are used. These are based on the experimentally determined cell numbers. For each experimental dataset, 10,000 simulations are performed, in which a number of cells corresponding to the experimentally found cells is randomly distributed over the same image areas. For each simulation run, the spatial statistics (Voronoi mesh, neighborhood, and cell cluster features) are computed in same way as for the experimental data. The results of all simulations are then compared with the "original," experimentally obtained data. To this end, the ratio is formed between the number of simulations in which the average cluster size is larger than in the experimental data and the total number of Monte Carlo simulations. This yields P values that indicate the probability that experimentally observed clusters could have been achieved by random cell distribution. For more details, see Ghigo et al. (2013).

Online supplemental material

Fig. S1, related to Fig. 1, shows the gating strategies exploited to identify epidermal DETCs and LCs as well as representative flow cytometry data for BM chimeric and parabiotic mice.

Acknowledgments

We thank the Centre d'Immunologie de Marseille-Luminy core facilities for animal housing, flow cytometry, and imaging (Plateforme d'Imagerie Commune du Site de Luminy, ImagImm, member of the national infrastructure France-BioImaging, supported by the French National Research Agency, ANR-10-INBS-04).

This study was funded by grants from the Agence National pour la Recherche (ANR-10-INBS-04-01 France-BioImaging, ANR-08-JCJC-0134). Additional support was provided by institutional grants from Institut National de la Santé et de la Recherche Médicale, Centre National de la Recherche Scientifique, and Aix-Marseille University to the Centre d'Immunologie de Marseille-Luminy. F. Ginhoux is a European Molecular Biology Organization Young Investigators Programme awardee and is supported by Singapore Immunology Network core funding as well as a Singapore National Research Foundation Senior Investigatorship (NRF2016NRF-NRFI001-02).

The authors declare no competing financial interests.

Author contributions: M. Bajénoff, R. Gentek, F. Ginhoux, and C. Ghigo designed the study. R. Gentek and M. Bajénoff wrote the manuscript. R. Gentek, C. Ghigo, G. Hoeffel, A. Jorquera, R. Msallam, S, Wienert, F. Klauschen, and M. Bajénoff performed and analyzed experiments. F. Ginhoux and G. Hoeffel edited the manuscript.

Submitted: 27 June 2018
Revised: 13 September 2018
Accepted: 23 October 2018

References

Almeida, F.F., M. Tenno, J. Brzostek, J.L. Li, G. Allies, G. Hoeffel, P. See, L.G. Ng, H.J. Fehling, N.R.J. Gascoigne, et al. 2015. Identification of a novel lymphoid population in the murine epidermis. *Sci. Rep.* 5:12554. https://doi.org/10.1038/srep12554

Asarnow, D.M., W.A. Kuziel, M. Bonyhadi, R.E. Tigelaar, P.W. Tucker, and J.P. Allison. 1988. Limited diversity of gamma delta antigen receptor genes of Thy-1+ dendritic epidermal cells. *Cell.* 55:837–847. https://doi.org/10.1016/0092-8674(88)90139-0

Baratin, M., L. Simon, A. Jorquera, C. Ghigo, D. Dembele, J. Nowak, R. Gentek, S. Wienert, F. Klauschen, B. Malissen, et al. 2017. T Cell Zone Resident Macrophages Silently Dispose of Apoptotic Cells in the Lymph Node. *Immunity.* 47:349–362.e5. https://doi.org/10.1016/j.immuni.2017.07.019

Bell, J.J., and A. Bhandoola. 2008. The earliest thymic progenitors for T cells possess myeloid lineage potential. *Nature.* 452:764–767. https://doi.org/10.1038/nature06840

Bergstresser, P.R., R.E. Tigelaar, J.H. Dees, and J.W. Streilein. 1983. Thy-1 antigen-bearing dendritic cells populate murine epidermis. *J. Invest. Dermatol.* 81:286–288. https://doi.org/10.1111/1523-1747.ep12518332

Böiers, C., J. Carrelha, M. Lutteropp, S. Luc, J.C.A. Green, E. Azzoni, P.S. Woll, A.J. Mead, A. Hultquist, G. Swiers, et al. 2013. Lymphomyeloid contribution of an immune-restricted progenitor emerging prior to definitive hematopoietic stem cells. *Cell Stem Cell.* 13:535–548. https://doi.org/10.1016/j.stem.2013.08.012

Boisset, J.-C., W. van Cappellen, C. Andrieu-Soler, N. Galjart, E. Dzierzak, and C. Robin. 2010. In vivo imaging of haematopoietic cells emerging from the mouse aortic endothelium. *Nature.* 464:116–120. https://doi.org/10.1038/nature08764

Breier, G., F. Breviario, L. Caveda, R. Berthier, H. Schnürch, U. Gotsch, D. Vestweber, W. Risau, and E. Dejana. 1996. Molecular cloning and expression of murine vascular endothelial-cadherin in early stage development of cardiovascular system. *Blood.* 87:630–641.

Cahalan, M.D., I. Parker, S.H. Wei, and M.J. Miller. 2002. Two-photon tissue imaging: seeing the immune system in a fresh light. *Nat. Rev. Immunol.* 2:872–880. https://doi.org/10.1038/nri935

Chodaczek, G., V. Papanna, M.A. Zal, and T. Zal. 2012. Body-barrier surveillance by epidermal γδ TCRs. *Nat. Immunol.* 13:272–282. https://doi.org/10.1038/ni.2240

Chorro, L., A. Sarde, M. Li, K.J. Woollard, P. Chambon, B. Malissen, A. Kissenpfennig, J.-B. Barbaroux, R. Groves, and F. Geissmann. 2009. Langerhans cell (LC) proliferation mediates neonatal development, homeostasis, and inflammation-associated expansion of the epidermal LC network. *J. Exp. Med.* 206:3089–3100. https://doi.org/10.1084/jem.20091586

Elbe, A., E. Tschachler, G. Steiner, A. Binder, K. Wolff, and G. Stingl. 1989. Maturational steps of bone marrow-derived dendritic murine epidermal cells. Phenotypic and functional studies on Langerhans cells and Thy-1+ dendritic epidermal cells in the perinatal period. *J. Immunol.* 143:2431–2438.

Elbe, A., O. Kilgus, R. Strohal, E. Payer, S. Schreiber, and G. Stingl. 1992. Fetal skin: a site of dendritic epidermal T cell development. *J. Immunol.* 149:1694–1701.

Fainaru, O., E. Woolf, J. Lotem, M. Yarmus, O. Brenner, D. Goldenberg, V. Negreanu, Y. Bernstein, D. Levanon, S. Jung, and Y. Groner. 2004. Runx3 regulates mouse TGF-beta-mediated dendritic cell function and its absence results in airway inflammation. *EMBO J.* 23:969–979. https://doi.org/10.1038/sj.emboj.7600085

Fainaru, O., D. Shseyov, S. Hantisteanu, and Y. Groner. 2005. Accelerated chemokine receptor 7-mediated dendritic cell migration in Runx3 knockout mice and the spontaneous development of asthma-like disease. *Proc. Natl. Acad. Sci. USA.* 102:10598–10603. https://doi.org/10.1073/pnas.0504787102

Gentek, R., C. Ghigo, G. Hoeffel, M.J. Bulle, R. Msallam, G. Gautier, P. Launay, J. Chen, F. Ginhoux, and M. Bajénoff. 2018. Hemogenic Endothelial Fate Mapping Reveals Dual Developmental Origin of Mast Cells. *Immunity.* 48:1160–1171.e5. https://doi.org/10.1016/j.immuni.2018.04.025

Ghigo, C., I. Mondor, A. Jorquera, J. Nowak, S. Wienert, S.P. Zahner, B.E. Clausen, H. Luche, B. Malissen, F. Klauschen, and M. Bajénoff. 2013. Multicolor fate mapping of Langerhans cell homeostasis. *J. Exp. Med.* 210:1657–1664. https://doi.org/10.1084/jem.20130403

Ginhoux, F., M. Greter, M. Leboeuf, S. Nandi, P. See, S. Gokhan, M.F. Mehler, S.J. Conway, L.G. Ng, E.R. Stanley, et al. 2010. Fate mapping analysis reveals that adult microglia derive from primitive macrophages. *Science.* 330:841–845. https://doi.org/10.1126/science.1194637

Girardi, M., J. Lewis, E. Glusac, R.B. Filler, L. Geng, A.C. Hayday, and R.E. Tigelaar. 2002. Resident skin-specific gammadelta T cells provide local, nonredundant regulation of cutaneous inflammation. *J. Exp. Med.* 195:855–867. https://doi.org/10.1084/jem.20012000

Girardi, M., E. Glusac, R.B. Filler, S.J. Roberts, I. Propperova, J. Lewis, R.E. Tigelaar, and A.C. Hayday. 2003. The distinct contributions of murine T cell receptor (TCR)gammadelta+ and TCRalphabeta+ T cells to different stages of chemically induced skin cancer. *J. Exp. Med.* 198:747–755. https://doi.org/10.1084/jem.20021282

Gomez Perdiguero, E., K. Klapproth, C. Schulz, K. Busch, E. Azzoni, L. Crozet, H. Garner, C. Trouillet, M.F. de Bruijn, F. Geissmann, and H.-R. Rodewald. 2015. Tissue-resident macrophages originate from yolk-sac-derived erythro-myeloid progenitors. *Nature.* 518:547–551. https://doi.org/10.1038/nature13989

Greter, M., I. Lelios, P. Pelczar, G. Hoeffel, J. Price, M. Leboeuf, T.M. Kündig, K. Frei, F. Ginhoux, M. Merad, and B. Becher. 2012. Stroma-derived interleukin-34 controls the development and maintenance of langerhans cells and the maintenance of microglia. *Immunity.* 37:1050–1060. https://doi.org/10.1016/j.immuni.2012.11.001

Hadjieconomou, D., S. Rotkopf, C. Alexandre, D.M. Bell, B.J. Dickson, and I. Salecker. 2011. Flybow: genetic multicolor cell labeling for neural circuit analysis in Drosophila melanogaster. *Nat. Methods.* 8:260–266. https://doi.org/10.1038/nmeth.1567

Hampel, S., P. Chung, C.E. McKellar, D. Hall, L.L. Looger, and J.H. Simpson. 2011. Drosophila Brainbow: a recombinase-based fluorescence labeling technique to subdivide neural expression patterns. *Nat. Methods.* 8:253–259. https://doi.org/10.1038/nmeth.1566

Havran, W.L., and J.P. Allison. 1988. Developmentally ordered appearance of thymocytes expressing different T-cell antigen receptors. *Nature.* 335:443–445. https://doi.org/10.1038/335443a0

Havran, W.L., and J.P. Allison. 1990. Origin of Thy-1+ dendritic epidermal cells of adult mice from fetal thymic precursors. *Nature.* 344:68–70. https://doi.org/10.1038/344068a0

Havran, W.L., and J.M. Jameson. 2010. Epidermal T cells and wound healing. *J. Immunol.* 184:5423–5428. https://doi.org/10.4049/jimmunol.0902733

Havran, W.L., S. Grell, G. Duwe, J. Kimura, A. Wilson, A.M. Kruisbeek, R.L. O'Brien, W. Born, R.E. Tigelaar, and J.P. Allison. 1989. Limited diversity of T-cell receptor gamma-chain expression of murine Thy-1+ dendritic epidermal cells revealed by V gamma 3-specific monoclonal antibody. *Proc. Natl. Acad. Sci. USA.* 86:4185–4189. https://doi.org/10.1073/pnas.86.11.4185

Havran, W.L., Y.H. Chien, and J.P. Allison. 1991. Recognition of self antigens by skin-derived T cells with invariant gamma delta antigen receptors. *Science.* 252:1430–1432. https://doi.org/10.1126/science.1828619

Heilig, J.S., and S. Tonegawa. 1986. Diversity of murine gamma genes and expression in fetal and adult T lymphocytes. *Nature.* 322:836–840. https://doi.org/10.1038/322836a0

Hoeffel, G., Y. Wang, M. Greter, P. See, P. Teo, B. Malleret, M. Leboeuf, D. Low, G. Oller, F. Almeida, et al. 2012. Adult Langerhans cells derive predominantly from embryonic fetal liver monocytes with a minor contribution of yolk sac-derived macrophages. *J. Exp. Med.* 209:1167–1181. https://doi.org/10.1084/jem.20120340

Hoeffel, G., J. Chen, Y. Lavin, D. Low, F.F. Almeida, P. See, A.E. Beaudin, J. Lum, I. Low, E.C. Forsberg, et al. 2015. C-Myb(+) erythro-myeloid progenitor-derived fetal monocytes give rise to adult tissue-resident macrophages. *Immunity.* 42:665–678. https://doi.org/10.1016/j.immuni.2015.03.011

Holzmann, S., C.H. Tripp, M. Schmuth, K. Janke, F. Koch, S. Saeland, P. Stoitzner, and N. Romani. 2004. A model system using tape stripping for characterization of Langerhans cell-precursors in vivo. *J. Invest. Dermatol.* 122:1165–1174. https://doi.org/10.1111/j.0022-202X.2004.22520.x

Honjo, M., A. Elbe, G. Steiner, I. Assmann, K. Wolff, and G. Stingl. 1990. Thymus-independent generation of Thy-1+ epidermal cells from a pool of Thy-1- bone marrow precursors. *J. Invest. Dermatol.* 95:562–567. https://doi.org/10.1111/1523-1747.ep12505543

Jameson, J., K. Ugarte, N. Chen, P. Yachi, E. Fuchs, R. Boismenu, and W.L. Havran. 2002. A role for skin gammadelta T cells in wound repair. *Science.* 296:747–749. https://doi.org/10.1126/science.1069639

Jameson, J.M., G. Cauvi, D.A. Witherden, and W.L. Havran. 2004. A keratinocyte-responsive gamma delta TCR is necessary for dendritic epidermal T cell activation by damaged keratinocytes and maintenance in the epidermis. *J. Immunol.* 172:3573–3579. https://doi.org/10.4049/jimmunol.172.6.3573

Jotereau, F., F. Heuze, V. Salomon-Vie, and H. Gascan. 1987. Cell kinetics in the fetal mouse thymus: precursor cell input, proliferation, and emigration. *J. Immunol.* 138:1026–1030.

Jung, S., J. Aliberti, P. Graemmel, M.J. Sunshine, G.W. Kreutzberg, A. Sher, and D.R. Littman. 2000. Analysis of fractalkine receptor CX(3)CR1 function by targeted deletion and green fluorescent protein reporter gene insertion. *Mol. Cell. Biol.* 20:4106–4114. https://doi.org/10.1128/MCB.20.11.4106-4114.2000

Kamath, A.T., S. Henri, F. Battye, D.F. Tough, and K. Shortman. 2002. Developmental kinetics and lifespan of dendritic cells in mouse lymphoid organs. *Blood.* 100:1734–1741.

Kamran, P., K.-I. Sereti, P. Zhao, S.R. Ali, I.L. Weissman, and R. Ardehali. 2013. Parabiosis in mice: a detailed protocol. *J. Vis. Exp.* (80). https://doi.org/10.3791/50556

Livet, J., T.A. Weissman, H. Kang, R.W. Draft, J. Lu, R.A. Bennis, J.R. Sanes, and J.W. Lichtman. 2007. Transgenic strategies for combinatorial expression of fluorescent proteins in the nervous system. *Nature.* 450:56–62. https://doi.org/10.1038/nature06293

MacLeod, A.S., R. Rudolph, R. Corriden, I. Ye, O. Garijo, and W.L. Havran. 2014. Skin-resident T cells sense ultraviolet radiation-induced injury and contribute to DNA repair. *J. Immunol.* 192:5695–5702.

Madisen, L., T.A. Zwingman, S.M. Sunkin, S.W. Oh, H.A. Zariwala, H. Gu, L.L. Ng, R.D. Palmiter, M.J. Hawrylycz, A.R. Jones, et al. 2010. A robust and high-throughput Cre reporting and characterization system for the whole mouse brain. *Nat. Neurosci.* 13:133–140. https://doi.org/10.1038/nn.2467

Mass, E., I. Ballesteros, M. Farlik, F. Halbritter, P. Günther, L. Crozet, C.E. Jacome-Galarza, K. Händler, J. Klughammer, Y. Kobayashi, et al. 2016. Specification of tissue-resident macrophages during organogenesis. *Science.* 353:aaf4238.

Masuda, K., M. Itoi, T. Amagai, N. Minato, Y. Katsura, and H. Kawamoto. 2005. Thymic anlage is colonized by progenitors restricted to T, NK, and dendritic cell lineages. *J. Immunol.* 174:2525–2532. https://doi.org/10.4049/jimmunol.174.5.2525

Matsue, H., P.R. Bergstresser, and A. Takashima. 1993. Keratinocyte-derived IL-7 serves as a growth factor for dendritic epidermal T cells in mice. *J. Immunol.* 151:6012–6019.

Merad, M., M.G. Manz, H. Karsunky, A. Wagers, W. Peters, I. Charo, I.L. Weissman, J.G. Cyster, and E.G. Engleman. 2002. Langerhans cells renew in the skin throughout life under steady-state conditions. *Nat. Immunol.* 3:1135–1141. https://doi.org/10.1038/ni852

Merad, M., F. Ginhoux, and M. Collin. 2008. Origin, homeostasis and function of Langerhans cells and other langerin-expressing dendritic cells. *Nat. Rev. Immunol.* 8:935–947. https://doi.org/10.1038/nri2455

Mondor, I., A. Jorquera, C. Sene, S. Adriouch, R.H. Adams, B. Zhou, S. Wienert, F. Klauschen, and M. Bajénoff. 2016. Clonal Proliferation and Stochastic

Pruning Orchestrate Lymph Node Vasculature Remodeling. *Immunity.* 45:877–888. https://doi.org/10.1016/j.immuni.2016.09.017

Orkin, S.H., and L.I. Zon. 2008. Hematopoiesis: an evolving paradigm for stem cell biology. *Cell.* 132:631–644. https://doi.org/10.1016/j.cell.2008.01.025

Palacios, R., and B.A. Imhof. 1993. At day 8-8.5 of mouse development the yolk sac, not the embryo proper, has lymphoid precursor potential in vivo and in vitro. *Proc. Natl. Acad. Sci. USA.* 90:6581–6585. https://doi.org/10.1073/pnas.90.14.6581

Palis, J., S. Robertson, M. Kennedy, C. Wall, and G. Keller. 1999. Development of erythroid and myeloid progenitors in the yolk sac and embryo proper of the mouse. *Development.* 126:5073–5084.

Pan, Y.A., T. Freundlich, T.A. Weissman, D. Schoppik, X.C. Wang, S. Zimmerman, B. Ciruna, J.R. Sanes, J.W. Lichtman, and A.F. Schier. 2013. Zebrabow: multispectral cell labeling for cell tracing and lineage analysis in zebrafish. *Development.* 140:2835–2846. https://doi.org/10.1242/dev.094631

Payer, E., A. Elbe, and G. Stingl. 1991. Circulating CD3+/T cell receptor V gamma 3+ fetal murine thymocytes home to the skin and give rise to proliferating dendritic epidermal T cells. *J. Immunol.* 146:2536–2543.

Samokhvalov, I.M., N.I. Samokhvalova, and S. Nishikawa. 2007. Cell tracing shows the contribution of the yolk sac to adult haematopoiesis. *Nature.* 446:1056–1061. https://doi.org/10.1038/nature05725

Sawai, C.M., S. Babovic, S. Upadhaya, D.J.H.F. Knapp, Y. Lavin, C.M. Lau, A. Goloborodko, J. Feng, J. Fujisaki, L. Ding, et al. 2016. Hematopoietic Stem Cells Are the Major Source of Multilineage Hematopoiesis in Adult Animals. *Immunity.* 45:597–609. https://doi.org/10.1016/j.immuni.2016.08.007

Scott, C.L., F. Zheng, P. De Baetselier, L. Martens, Y. Saeys, S. De Prijck, S. Lippens, C. Abels, S. Schoonooghe, G. Raes, et al. 2016. Bone marrow-derived monocytes give rise to self-renewing and fully differentiated Kupffer cells. *Nat. Commun.* 7:10321. https://doi.org/10.1038/ncomms10321

Sharp, L.L., J.M. Jameson, G. Cauvi, and W.L. Havran. 2005. Dendritic epidermal T cells regulate skin homeostasis through local production of insulin-like growth factor 1. *Nat. Immunol.* 6:73–79.

Sörensen, I., R.H. Adams, and A. Gossler. 2009. DLL1-mediated Notch activation regulates endothelial identity in mouse fetal arteries. *Blood.* 113:5680–5688. https://doi.org/10.1182/blood-2008-08-174508

Strid, J., O. Sobolev, B. Zafirova, B. Polic, and A. Hayday. 2011. The intraepithelial T cell response to NKG2D-ligands links lymphoid stress surveillance to atopy. *Science.* 334:1293–1297.

Sumaria, N., B. Roediger, L.G. Ng, J. Qin, R. Pinto, L.L. Cavanagh, E. Shklovskaya, B. Fazekas de St Groth, J.A. Triccas, and W. Weninger. 2011. Cutaneous immunosurveillance by self-renewing dermal gammadelta T cells. *J. Exp. Med.* 208:505–518. https://doi.org/10.1084/jem.20101824

Wang, Y., K.J. Szretter, W. Vermi, S. Gilfillan, C. Rossini, M. Cella, A.D. Barrow, M.S. Diamond, and M. Colonna. 2012. IL-34 is a tissue-restricted ligand of CSF1R required for the development of Langerhans cells and microglia. *Nat. Immunol.* 13:753–760. https://doi.org/10.1038/ni.2360

Waskow, C. 2010. Generation of parabiotic mice for the study of DC and DC precursor circulation. *Methods Mol. Biol.* 595:413–428. https://doi.org/10.1007/978-1-60761-421-0_27

Woolf, E., O. Brenner, D. Goldenberg, D. Levanon, and Y. Groner. 2007. Runx3 regulates dendritic epidermal T cell development. *Dev. Biol.* 303:703–714. https://doi.org/10.1016/j.ydbio.2006.12.005

Ye, S.K., K. Maki, H.C. Lee, A. Ito, K. Kawai, H. Suzuki, T.W. Mak, Y. Chien, T. Honjo, and K. Ikuta. 2001. Differential roles of cytokine receptors in the development of epidermal gamma delta T cells. *J. Immunol.* 167:1929–1934. https://doi.org/10.4049/jimmunol.167.4.1929

Yona, S., K.W. Kim, Y. Wolf, A. Mildner, D. Varol, M. Breker, D. Strauss-Ayali, S. Viukov, M. Guilliams, A. Misharin, et al. 2013. Fate mapping reveals origins and dynamics of monocytes and tissue macrophages under homeostasis. *Immunity.* 38:79–91. https://doi.org/10.1016/j.immuni.2012.12.001

Yoshimoto, M., P. Porayette, N.L. Glosson, S.J. Conway, N. Carlesso, A.A. Cardoso, M.H. Kaplan, and M.C. Yoder. 2012. Autonomous murine T-cell progenitor production in the extra-embryonic yolk sac before HSC emergence. *Blood.* 119:5706–5714. https://doi.org/10.1182/blood-2011-12-397489

Zovein, A.C., J.J. Hofmann, M. Lynch, W.J. French, K.A. Turlo, Y. Yang, M.S. Becker, L. Zanetta, E. Dejana, J.C. Gasson, et al. 2008. Fate tracing reveals the endothelial origin of hematopoietic stem cells. *Cell Stem Cell.* 3:625–636. https://doi.org/10.1016/j.stem.2008.09.018